Intrinsically organized resting state networks in the human spinal cord

Yazhuo Kong[a,1,2], Falk Eippert[a,b,1], Christian F. Beckmann[a,c], Jesper Andersson[a], Jürgen Finsterbusch[b], Christian Büchel[b], Irene Tracey[a], and Jonathan C. W. Brooks[d]

[a]Oxford Centre for Functional Magnetic Resonance Imaging of the Brain, Nuffield Department of Clinical Neurosciences, University of Oxford, Oxford OX3 9DU, United Kingdom; [b]Department of Systems Neuroscience, University Medical Center Hamburg-Eppendorf, Hamburg 20246, Germany; [c]Donders Institute for Brain, Cognition and Behaviour, Radboud University Nijmegen, and Department of Cognitive Neuroscience, Radboud University Medical Centre, Nijmegen 6500 HB, The Netherlands; and [d]Clinical Research and Imaging Centre, University of Bristol, Bristol BS2 8DX, United Kingdom

Edited by Marcus E. Raichle, Washington University in St. Louis, St. Louis, MO, and approved November 11, 2014 (received for review July 27, 2014)

Spontaneous fluctuations in functional magnetic resonance imaging (fMRI) signals of the brain have repeatedly been observed when no task or external stimulation is present. These fluctuations likely reflect baseline neuronal activity of the brain and correspond to functionally relevant resting-state networks (RSN). It is not known however, whether intrinsically organized and spatially circumscribed RSNs also exist in the spinal cord, the brain's principal sensorimotor interface with the body. Here, we use recent advances in spinal fMRI methodology and independent component analysis to answer this question in healthy human volunteers. We identified spatially distinct RSNs in the human spinal cord that were clearly separated into dorsal and ventral components, mirroring the functional neuroanatomy of the spinal cord and likely reflecting sensory and motor processing. Interestingly, dorsal (sensory) RSNs were separated into right and left components, presumably related to ongoing hemibody processing of somatosensory information, whereas ventral (motor) RSNs were bilateral, possibly related to commissural interneuronal networks involved in central pattern generation. Importantly, all of these RSNs showed a restricted spatial extent along the spinal cord and likely conform to the spinal cord's functionally relevant segmental organization. Although the spatial and temporal properties of the dorsal and ventral RSNs were found to be significantly different, these networks showed significant interactions with each other at the segmental level. Together, our data demonstrate that intrinsically highly organized resting-state fluctuations exist in the human spinal cord and are thus a hallmark of the entire central nervous system.

fMRI | spinal cord | resting state | connectivity | networks

Functional magnetic resonance imaging (fMRI) has been used to study the functional connectivity of the human brain, with spontaneous fluctuations in the resting-state fMRI signal (1–3) attracting much attention in the past few years (for review, see refs. 4–6). Brain regions showing temporally coherent spontaneous fluctuations constitute several anatomically consistent "resting state networks" (RSNs), such as visual, auditory, sensorymotor, executive control, and default mode networks (7–11). Consequently, analyses of RSNs are rapidly emerging as a powerful tool for in vivo mapping of neural circuitry in the human brain and one such approach for exploring RSNs is independent component analysis (ICA) (12–14). ICA decomposes the data into spatially independent and temporally coherent source signals/components. The advantage of ICA over more traditional seed-based approaches (15) is that it is a model-free, data-driven multiple-regression approach, i.e., within the ICA framework we can account for multiple underlying signal contributions (artifactual or neuronal in origin) simultaneously and thereby disentangle these different contributions to the measured observations (16). To date, ICA has been used not only to characterize brain connectivity in healthy adults (7, 10, 17), but also to assess the development of brain connectivity at various stages of (18, 19) as well as across the lifespan (20) and to investigate connectivity alterations in clinical populations (21–24).

Here, we use this approach to investigate the intrinsic organization of RSNs in the human spinal cord. The spinal cord is the first part of the central nervous system (CNS) involved in the transmission of somatosensory information from the body periphery to the brain, as well as the last part of the CNS involved in relaying motor signals to the body periphery. This functional separation is also evident in the anatomical organization of the spinal cord, with the ventral part of gray matter involved in motor function and the dorsal part involved in somatosensory processing. The corresponding pairs of ventral and dorsal nerve roots convey information to and from the body periphery with a rostro-caudal topographical arrangement for both sensory (dermatomes) and motor innervation (myotomes).

Although such a precise anatomical layout would suggest clear organizational principles for intrinsic spinal cord networks (similar to e.g., the visual and auditory RSNs in the brain), it is not known whether spatially consistent RSNs exist in the spinal cord. Distinct spatial maps due to cardiac and respiratory noise sources have been revealed by single subject ICA (25–27), and a seed-based approach demonstrated correlations between ventral horns and between dorsal horns (28), but no group patterns of circumscribed motor or sensory networks have yet been found; also only a few investigations of task-based functional connectivity have been performed (29–31). One reason for the apparent lack

Significance

The human brain displays an enormous amount of intrinsic activity in the absence of any task or external stimulation. Here we demonstrate that the human spinal cord, the brain's principal interface with the body, also shows such resting-state activity. We observed biologically plausible and spatially distinct networks that reflect the functional organisation of the spinal cord: networks in the anterior part likely relating to motor function and distinct networks in the posterior part likely reflecting sensory function. These networks were grouped along the spinal cord, consistent with motor output to, and sensory input from, the body. Together with previous brain imaging studies, our data suggest that resting-state activity constitutes a major functional signature of the entire central nervous system.

Author contributions: Y.K., F.E., J.F., C.B., I.T., and J.C.W.B. designed research; Y.K., F.E., and J.C.W.B. performed research; C.F.B., J.A., and J.F. contributed new reagents/analytic tools; Y.K., F.E., C.F.B., J.A., and J.C.W.B. analyzed data; and Y.K., F.E., C.B., I.T., and J.C.W.B. wrote the paper.

The authors declare no conflict of interest.

This article is a PNAS Direct Submission.

[1]Y.K. and F.E. contributed equally to this work.

[2]To whom correspondence should be addressed. Email: yazhuo.kong@ndcn.ox.ac.uk.

This article contains supporting information online at www.pnas.org/lookup/suppl/doi:10.1073/pnas.1414293111/-/DCSupplemental.

NEUROSCIENCE

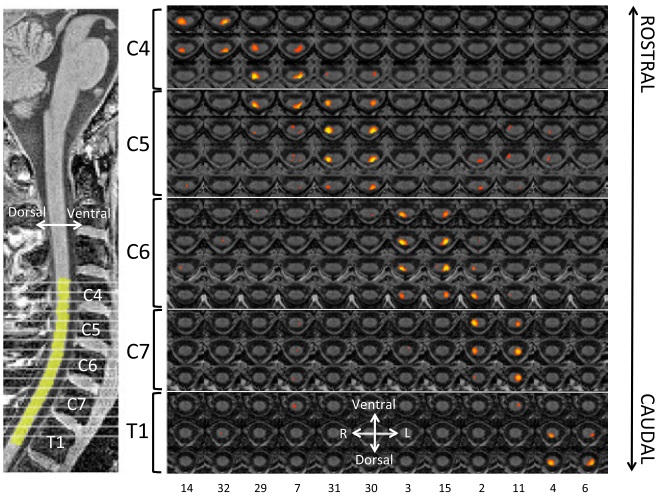

Fig. 1. Dorsal (sensory) RSNs. These networks were identified using a group ICA in a restricted region that just included the spinal cord. (*Left*) A sagittal section of our T1-weighted template depicting the location of the displayed transversal sections (gray lines) from C4 to T1 as well as the excellent overlap with the group spinal cord mask (yellow). (*Right*) The dorsal RSNs are arranged in anatomical level order with each column corresponding to one component. Both the restricted rostro-caudal extension of each component and the unilateral occurrence are clearly evident. Each RSN map is thresholded at FDR $P < 0.05$ and shown in rostral-caudal direction with the component ranking number at the bottom. Note that component ordering is based on the amount of variance each component explains (in decreasing order).

of relevant data is that fMRI is more challenging to perform in the spinal cord than in the brain (32, 33). The difficulties faced are mostly due to its small cross-sectional area (~1 cm^2, necessitating the use of small voxel sizes, which leads to a low signal-to-noise ratio), magnetic susceptibility differences in tissues adjacent to the cord, e.g., vertebral bodies and spinous processes (causing signal loss and image distortion), as well as the influence of physiological noise (obscuring neuronally induced signal changes).

Here, we used recent improvements in spinal fMRI [i.e., acquisition techniques that mitigate magnetic susceptibility differences (34), validated procedures for physiological noise reduction (35, 36) and techniques that allow voxel-wise group analyses (37, 38)] to overcome these difficulties and investigate the organizational principles of RSNs in the human spinal cord. We hypothesized that dorsal and ventral regions of the spinal cord would show different patterns of resting activity and furthermore investigated whether the segmental organization of the spinal cord would be evident in the rostro-caudal spatial layout of spinal RSNs.

Results

Data Quality. *SI Appendix*, Fig. S1 shows the power spectrum of spinal cord fMRI time courses averaged across all participants during different steps of our data-processing pipeline. After motion correction, spinal cord data (solid blue line) remains noisy, with power spread across the entire frequency range, unlike the low-frequency fluctuations (<0.1 Hz) commonly observed in resting state BOLD signals in the brain. One possible reason for this might be the presence of physiological noise (mainly of cardiac and respiratory origin), which is a major source of signal variance in the spinal cord. The power spectrum was rather similar after high-pass filtering and spatial smoothing (dashed green line), which mainly removed very low frequency drift. However, the application of a validated physiological noise model (red line) worked reasonably well in attenuating the aliased physiological noise.

As all of the following analyses are carried out in a common anatomical space, the results critically depend on the accuracy of intersubject registration. To demonstrate the accuracy of our registration procedure, hand-drawn spinal cord masks based on the functional data of each individual were registered to our spinal cord template and averaged up to generate a group cord mask, which only consisted of voxels that were included in every single participant's mask. The overlap of this conservative group cord mask with the spinal cord template was excellent (Figs. 1 and 2, *Left*). Individual results from spatial normalization are presented in *SI Appendix*, Fig. S2, which demonstrates excellent agreement between the cord outline and the chosen template.

Spatial Distribution of Spinal Resting State Networks (RSNs). To identify spinal cord networks, we used the standard approach of group concatenation ICA (12), which resulted in 40 spatially independent networks within the group cord mask, all of which are FDR-corrected at a threshold of $P < 0.05$. Based on visual inspection of each component's spatial profile, we classified these networks as either dorsal "sensory" networks (12 components; Fig. 1), ventral "motor" networks (12 components; Fig. 2), or networks of no interest (*SI Appendix*, Fig. S3). The latter category mainly consisted of components with a very central spatial profile, which most likely reflect residual CSF fluctuations in the central canal of the spinal cord (situated in the middle of the cord); there were also a few components that spanned the dorsal and ventral part of the spine. The rostro-caudal extension of all RSNs (sensory, motor and no interest) was relatively limited, as they almost never extended for more than one vertebral level, seemingly mirroring the anatomical organization of the spinal cord into circumscribed segments. Interestingly, the ventral RSNs were predominantly bilateral, whereas the dorsal

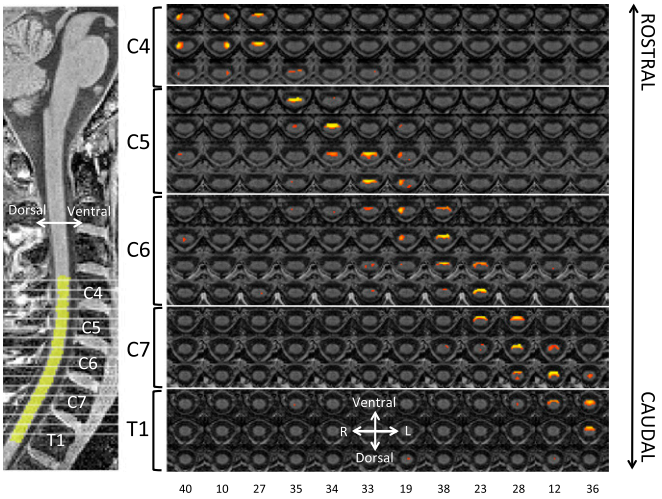

Fig. 2. Ventral (motor) RSNs. These networks were identified using a group ICA in a restricted region that just included the spinal cord. (*Left*) A sagittal section of our T1-weighted template depicting the location of the displayed transversal sections (gray lines) from C4 to T1 as well as the excellent overlap with the group spinal cord mask (yellow). (*Right*) The ventral RSNs are arranged in anatomical level order with each column corresponding to one component. Both the restricted rostro-caudal extension of each component and the mostly bilateral occurrence are clearly evident. Each RSN map is thresholded at FDR $P < 0.05$ and shown in rostral-caudal direction with the component ranking number at the bottom. Note that component ordering is based on the amount of variance each component explains (in decreasing order).

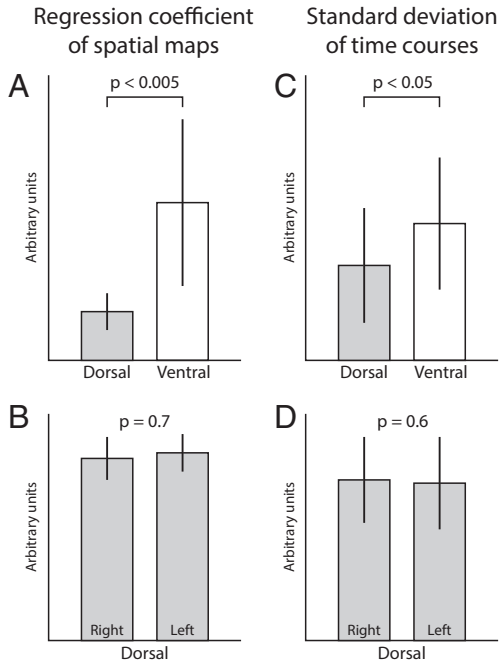

Fig. 3. Intrinsic properties of visually identified RSNs. Depicted are comparisons of the spatial map regression coefficients (representing the degree of coactivation) and the component time series SD (representing the component strength). We observed significant differences for both metrics between dorsal and ventral RSNs (*A* and *C*), but not between left and right dorsal RSNs (*B* and *D*); note that the laterality analysis could not be done for ventral RSNs as these were predominantly bilateral. Error bars represent standard deviation.

RSNs showed a clear tendency toward separation into lateralised components for the right and left dorsal horn.

Spatial Distribution of Spinal RSNs: Control Analyses. First, to eliminate the possibility that the observed bilaterality of the ventral RSNs is due to spatial smoothing (as the ventral horns are closer together than the dorsal horns), we repeated the above analysis on unsmoothed data. The pattern of bilateral ventral components remained in this analysis (*SI Appendix*, Fig. S4 and Table S1), so it is unlikely that the bilateral RSNs are an artifact of spatial smoothing. Second, to test whether the rostro-caudal extent of the components is influenced by the number of vertebral levels included in the analysis, we repeated our original analysis on levels C5-C7, i.e., discarding data from levels C4 and T1 before running the ICA. The results of these control analyses were very similar to our original results, with RSNs spanning approximately the same rostro-caudal distance (*SI Appendix*, Fig. S5 and Table S2), suggesting that the chosen approach indeed picks up anatomical information and that the observed RSNs are not due to methodological confounds. Third, to ensure that the observed RSNs were not contaminated by white matter signal, we regressed out this signal source before running the ICA in a further control analysis; this analysis produced very similar results (*SI Appendix*, Fig. S6 and Table S3) and suggests that white matter signal fluctuations contribute relatively little to the obtained results. Fourth, as our original analysis was restricted to the spinal cord region, there is a possibility that the identified components might be drawn from signal fluctuations in the surrounding CSF. We therefore ran an additional analysis within a larger region including the subarachnoid space surrounding the spinal cord and containing CSF. It can be seen that the main dorsal and ventral RSNs are primarily located within the spinal cord with limited extension into the CSF space (*SI Appendix*, Fig. S7 and Table S4), possibly due to effects of spatial smoothing. Importantly, the spatial configuration of these networks is distinct from components that were not selected as dorsal or ventral networks, most of which have a clear focus outside the spinal cord and are likely of artifactual origin (*SI Appendix*, Fig. S8).

Network Analysis. Next we applied a dual-regression technique (39), which provides each individual participant's RSN spatial maps and associated time courses, to investigate differences in the intrinsic properties of the visually identified ventral and dorsal RSNs. Therefore, we compared the spatial map regression coefficients (representing the degree of coactivation) and the component time series standard deviation (representing the component strength) between dorsal and ventral networks. We observed that both the degree of coactivation ($P = 0.000017$) and the component strength ($P = 0.0098$) were significantly higher for the ventral networks than for the dorsal networks (Fig. 3); there were no differences between left and right dorsal RSNs. This finding implies that, although the dorsal and ventral networks were identified visually using anatomical locations, these two network types showed significant differences in spatial and temporal properties.

Finally, we examined correlations between the time courses of all RSNs to characterize the relationships between these networks (Fig. 4). Within both dorsal and ventral RSNs, components are positively correlated at the same level but not correlated or even negatively correlated to other levels. Interestingly, dorsal and ventral networks are positively correlated at the same level (box in lower left corner of Fig. 4). Please note that the asterisks indicate correlations surviving stringent correction for multiple comparisons (FWE at $P < 0.05$ using nonparametric permutation testing). Althought these results were obtained using standard correlations (which can reflect both direct and indirect functional connections), we also used a partial correlation approach (which is more likely to reflect direct functional connections), the results of which

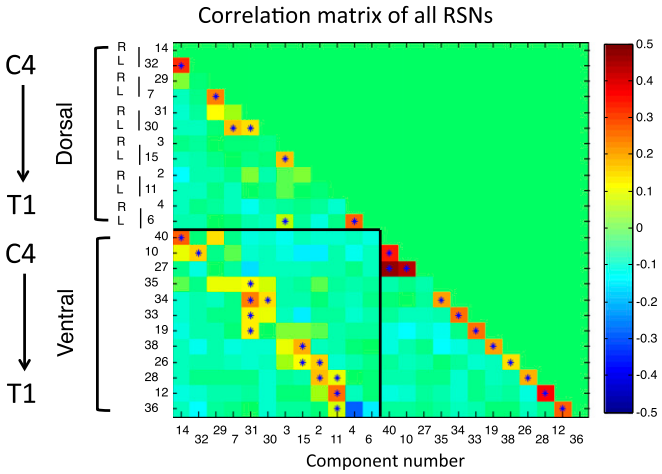

Fig. 4. RSN correlation matrix. This correlation matrix contains the full correlations between the time-courses of all visually identified dorsal and ventral components (see *SI Appendix*, Fig. S9 for partial correlations). Components were arranged in rostro-caudal anatomical order, similar to Figs. 1 and 2. For both dorsal and ventral RSNs, components are positively correlated at the same rostro-caudal level, but not correlated or even slightly negatively correlated to other levels. Interestingly, dorsal and ventral networks of the same level are positively correlated (box in lower left corner; except for T1 – component 4 and 36). Asterisks indicate correlations significant at $P < 0.05$ (FWE corrected using nonparametric permutation testing). Note that component ordering is based on the amount of variance each component explains (in decreasing order).

NEUROSCIENCE

showed a similar pattern, although correlations were more sparse and lower in amplitude (*SI Appendix*, Fig. S9).

Reliability and Reproducibility. To estimate the reliability of the observed dorsal and ventral spinal RSNs, we used a split-half method in combination with calculation of intraclass correlation coefficients (ICCs; ref. 40). Despite effectively halving the amount of data available for ICA, we observed that slightly more than half of the voxels making up the dorsal and ventral components showed at least fair reliability (52.7% of voxels with ICCs > 0.4), whereas around a quarter of the voxels showed at least good reliability (25.9% of voxels with ICCs > 0.6); there was a tendency for ventral networks to exhibit higher ICCs than dorsal networks (*SI Appendix*, Fig. S10 and Table S5). Similarly, the reproducibility of the observed RSNs at the individual subject level (as estimated via template-matching procedures, where we used group ICA and dual regression templates against single session individual ICA maps; *SI Appendix*, Fig. S11) exhibited spatial correlation coefficients of 0.4–0.8, with ventral networks showing a tendency for higher reproducibility.

Discussion

This fMRI study presents an extensive evaluation of whether consistent and spatially distinct resting state networks (RSNs) are detectable in the human spinal cord. Observed RSNs were intrinsically organized in pairs of dorsal sensory RSNs and bilateral ventral motor RSNs, and appear to reflect segmental input to, and output from, the cord. These results were obtained by combining several recent advancements in spinal cord fMRI to address the inherent difficulties in imaging this structure: signal loss due to periodic magnetic field inhomogeneities and partial voluming effects due to the small cross-sectional cord diameter were mitigated by using a tailored image acquisition protocol (34), physiological noise of respiratory and cardiac nature was reduced by using a validated physiological noise model (35, 36), and the low signal-to-noise level and interindividual differences in anatomy were addressed using group analysis techniques (37, 38).

The first noticeable feature of all spinal cord RSNs was their clearly circumscribed extent in the rostro-caudal direction, with almost no component extending for more than the length of about one vertebra. It is important to note that these RSNs were obtained using a completely model-free and data-driven technique (independent component analysis; ref. 12) and are thus an intrinsic feature of spinal cord organization. Once probabilistic atlases of the segmental organization of the spinal cord are published, it will be interesting to investigate whether the extent of these RSNs coincides with segmental borders or whether they adhere to some organizational principle that is independent of this traditional parcellation of the spinal cord. In this regard it is important to note that intersegmental connectivity could for example easily be realized via (*i*) shared peripheral input in the dorsal cord through axons extending rostro-caudally in Lissauer's tract and (*ii*) long-range propriospinal interneurons in the ventral part of the cord. However, we also observed that RSNs at different spinal cord levels were not correlated at all or even weakly anti-correlated, which is interesting in the light of intersegmental "lateral inhibition" in the dorsal part of the spinal cord during sensory processing (41) and intersegmental phase-lags in the ventral part of the spinal cord underlying motor coordination (42).

The second important feature of spinal cord RSNs was their separation into distinct dorsal and ventral components. This separation nicely mirrors the functional neuroanatomy of the spinal cord, with sensory processing occurring in the dorsal cord and motor processing occurring in the ventral cord. These distinct networks were observed using group concatenation ICA and dual regression. Although their identification was based on visual inspection of the data alone, these two types of components had clearly different intrinsic properties: both the degree of spatial coactivation and the temporal dynamics were significantly stronger in the ventral RSNs compared with the dorsal RSNs. Despite these significant differences in intrinsic properties, dorsal and ventral networks at the same rostro-caudal level showed a strong positive correlation with each other. It could be argued that spatial smoothing may drive these correlations, but because there were no positive correlations across different levels (where our anisotropic smoothing kernel should have the strongest effect) this seems rather unlikely.

A further difference between ventral and dorsal spinal RSNs was that ventral networks were predominantly bilateral, whereas dorsal networks were predominantly unilateral. This finding is interesting with regard to a seed-based resting-state study that observed stronger connectivity between ventral horns than dorsal horns (28) and two previous task-based spinal fMRI studies that showed a strong bilateral activation during motor tasks (43), but a clearly lateralized activation during painful sensory stimulation (37). Although such correspondence between task-related and resting-state spinal fMRI signals might be incidental, there is also evidence for a close correspondence of task-related and resting-state networks in the brain (10). Interestingly, the spatially separated unilateral dorsal sensory RSNs did not differ in their intrinsic properties (spatial coactivation and temporal dynamics).

The origin of these intrinsically organized fluctuations of spinal cord signals in the resting-state can obviously not be resolved with fMRI, but there are several (not mutually exclusive) explanations. A first possibility is that they are related to ongoing input from the body periphery, as the central nervous system is continuously receiving information about the state of the body (e.g., proprioceptive information regarding limb positions) and its interaction with the environment (e.g., tactile information regarding touch or pressure). Viewed in such a light, the unilateral dorsal components could reflect ongoing hemibody processing, consistent with the ipsilateral organization of sensory input. A second possibility is that the observed fluctuations reflect ongoing descending and ascending traffic, i.e., the communication with supraspinal structures involved in motor control and somatosensory feedback via the corticospinal tract and the spinothalamic tract for example. In the uppermost cervical parts we imaged, there is also the possibility that the components could reflect communication within a brainstem-phrenic nerve system involved in the control of respiration (44). Finally, there is the possibility that they reflect intrinsic fluctuations that are local to the spinal cord. It is well known that intrinsic neuronal networks in the mammalian spinal cord are capable of controlling the pattern of the muscle activity and producing rhythmic movements even when the spinal cord itself is isolated from the brain and sensory inputs. These self-organized spinal networks are called central pattern generators (CPGs) and underlie coordinated movements such as breathing and locomotion (45–47). The interneurons that make up these networks are known to be active at rest (ref. 48; see also ref. 49 for an example of slow rhythmic spinal fluctuations) and cervical intercommissural interneurons (50) might play a role in establishing the bilateral fluctuations that we observed in the motor-related ventral portion of the spinal cord. Interestingly, such bilateral resting-state fluctuations were also observed in the first-resting state study in the motor cortex (1). We would expect that the three potential mechanisms we list here for explaining spinal resting-state fluctuations continuously interact with each other to support both local demands and more global processes that involve constant communication with the brain.

Although it is conceivable that the presence of large draining veins on the ventral and dorsal surfaces of the cord might contribute to the observed patterns of resting signal fluctuation (51), several lines of evidence argue against this as an explanation for our results. First, we tailored fMRI acquisition parameters

to match the small dimensions of the cord (maximum diameter ~12mm; ref. 52), and thus used a relatively high resolution (1 mm in-plane). Although the point spread function (PSF) of the EPI acquisition is not negligible and will depend on the local T2* of the cord (which will vary along the cord), in this study we estimate that the PSF ranged from 1.2 to 1.7 times the specified resolution based on assumed T2* values of 50 and 25 ms (worst case), respectively. Second, the anisotropic smoothing kernel applied was chosen to mitigate such problems, by maximally integrating signal along the cord rather than across it. Indeed, by using a z-shimmed EPI acquisition (34) we have minimized through slice dephasing, reducing signal loss due to periodic susceptibility differences along the cord, and preserved cord shape across slices. Third, concerning the orientation of the major draining veins, which run parallel to the long axis of the cord, these are likely to be parallel to the main static magnetic field, and so should theoretically contribute little to recorded signal (53). By performing comprehensive slice-wise physiological noise removal, based on independent measurement of each subject's physiological signals, we have attempted to remove such confounding noise sources (primarily cardiac in origin) that have previously been observed near the surface of the cord with ICA based analysis (25, 35). It should be noted that our results also held when controlling for white matter signal, accounting for the influence of CSF, and when changing the rostro-caudal extent of the investigated volume; lastly, the identified components mostly showed fair to good intrasession reliability and reproducibility.

Previous studies of RSNs in the brain used either a predefined spatial template or visual inspection in combination with anatomical knowledge to define resting state networks (7). Here we followed the latter approach in identifying spinal RSNs, as no such spatial template exists for the spinal cord. It is therefore crucial to confirm in future studies whether the identified spinal cord RSNs could provide a spatial template for general-purpose use. Should this be the case, analyses of spinal RSNs could become an important tool in investigating clinical populations that involve spinal cord pathology, such as multiple sclerosis (54, 55) and spinal cord injury (56, 57) as well as the neuroplastic and sensitization changes known to occur in the spinal cord in various forms of chronic pain (58). A limitation of this study is that we used a restricted field of view that covered the spinal cord only from C4 to T1. It would obviously be desirable to extend the coverage and investigate resting-state activity along the whole spinal cord. Furthermore, because the spinal cord continuously interacts with numerous supraspinal structures to support sensory, motor and homeostatic processing, it would be desirable to use new image acquisition techniques to investigate the brain and spinal cord simultaneously (59). Such an approach could allow an investigation of wide-range resting-state connectivity and would result in a more integrative picture of central nervous system function.

Materials and Methods

Participants. The data reported here is part of a larger spinal fMRI project and an independent part of this data set (24 healthy male participants) has already been published (34). Due to problems with physiological data acquisition, data from 4 participants had to be discarded, resulting in a final sample size of 20 (age: 26.45 ± 3.9 y). The Ethics Committee of the Medical Board in Hamburg, Germany, approved the study and all participants gave written informed consent.

Data Acquisition. fMRI data were acquired in an eyes-open state on a 3 tesla system (Siemens Magnetom Trio, Siemens, Erlangen, Germany), using a recently developed sequence that (*i*) minimized signal dropout due to magnetic field inhomogeneities via slice-specific z-shimming and (*ii*) used nonisotropic voxels (1 × 1 × 5mm) to provide high in-plane resolution while retaining an adequate signal-to-noise ratio (34) (for details, see *SI Appendix, SI Materials and Methods*). A total of 250 volumes were acquired for each volunteer (7.5 min scanning time) with each volume covering the spinal cord from the fourth cervical vertebra to the first thoracic vertebra. To monitor cardiac and respiratory signals, participants wore a pulse oximeter and respiratory belt, and physiological data were recorded together with the trigger pulses preceding the acquisition of each volume.

Data Preprocessing. Data were preprocessed using tools from FSL (FMRIB Software Library, www.fmrib.ox.ac.uk/fsl). Each slice was motion corrected in 2D (translations only) using FLIRT (60). Please note that slice-wise motion correction is necessary, as spinal cord displacement varies along the rostro-caudal axis according to the cardiac (61) and respiratory cycle (62). Subsequently, data were spatially smoothed with an anisotropic kernel (2 × 2 × 8 mm FWHM) and high-pass temporal filtered (100-s cutoff). A significant challenge for spinal cord fMRI is the influence of physiological noise (primarily of cardiac and respiratory nature), which severely degrades data quality. To address this issue, we used a recently developed and validated physiological noise model (35, 36), which removes physiological confounds from motion corrected data using slice-specific regressors (for details, see *SI Appendix, SI Materials and Methods*) and the obtained residuals from each fMRI scan were used for further analysis. The residuals from each participant were then registered to the corresponding structural image and all images were brought into a common anatomical space to allow for group analysis (for details, see *SI Appendix, SI Materials and Methods*).

Data Analysis. First, we carried out a group independent component analysis (ICA) on the fMRI data using standard procedures as implemented in MELODIC (12). The functional data were temporally concatenated across participants to create a single 4D data set. A group ICA was then performed within the spinal cord area (using 40 independent components) and the resulting independent component spatial maps were FDR corrected ($P < 0.05$). RSNs of interest (dorsal and ventral networks) were selected visually, based on their anatomical location. We also performed several control analyses to rule out confounding factors and to establish the reliability and reproducibility of our approach (*SI Appendix, SI Materials and Methods*).

Next, we used a dual regression technique to obtain participant-specific component maps, along with associated time series (39). Specifically, for each participant the previously obtained group-ICA spatial maps were used as spatial regressors against each subject's 4D residual data, to estimate the weight of each component at each time point. Before being fed into the model, each component map was demeaned. This procedure resulted in one time series for each component. The obtained time series were then used as temporal regressors against each participant's preprocessed functional data, to estimate the individual participant-level spatial maps. Each time series was demeaned and normalized before entering the regression model.

Individual component maps and corresponding time-series from the dual regression analysis were then used to test for differences in the intrinsic properties of the visually identified RSNs. For dorsal and ventral RSNs, the individual spatial map regression coefficients, representing the degree of coactivation, were averaged and compared across all participants. Subsequently, the SDs from each corresponding component time-series (representing the component strength or amplitude), calculated before they were normalized for use as regressors in the second dual regression stage, were also compared for dorsal and ventral RSNs. The same comparisons were performed comparing right and left dorsal RSNs. In all cases paired *t* tests were used.

Finally, we estimated correlations between all RSN time series to characterize the relationship between those networks. This estimation was done in two ways, namely via the full correlation (CORR) and via the regularized normalized inverse of the covariance matrix (ICOV) (63, 64). CORR evaluates the similarity between two time series directly, and reflects both direct and indirect functional connections. ICOV, however, evaluates the similarity between two time series after regressing out the influences from all other time series, and is a regularized version of partial correlation – the resulting measure should emphasize direct, rather than indirect, functional connections (63). We use an ICOV implementation referred to as L1precision (www.cs.ubc.ca/~schmidtm/Software/L1precision.html), with the regularization-controlling parameter lambda of 5 (64). Significance testing of all correlation coefficients was performed using multiple comparison correction (FWE at $P < 0.05$ using nonparametric permutation testing with 5,000 permutations; ref. 65).

ACKNOWLEDGMENTS. Y.K. and J.C.W.B. were supported by the Medical Research Council (UK). F.E. was supported by a Marie Curie Fellowship (Grant 273805, "Pain modulation") and the Centre for Functional Magnetic Resonance Imaging of the Brain (IT) by the Wellcome Trust and Medical Research Council (UK). C.B. is supported by the Deutsche Forschungsgemeinschaft (FOR 1328 and SFB 936) and European Research Council (2010-AdG_20100407).

1. Biswal B, Yetkin FZ, Haughton VM, Hyde JS (1995) Functional connectivity in the motor cortex of resting human brain using echo-planar MRI. *Magn Reson Med* 34(4):537–541.
2. Lowe MJ, Mock BJ, Sorenson JA (1998) Functional connectivity in single and multislice echoplanar imaging using resting-state fluctuations. *Neuroimage* 7(2):119–132.
3. Cordes D, et al. (2000) Mapping functionally related regions of brain with functional connectivity MR imaging. *AJNR Am J Neuroradiol* 21(9):1636–1644.
4. Fox MD, Raichle ME (2007) Spontaneous fluctuations in brain activity observed with functional magnetic resonance imaging. *Nat Rev Neurosci* 8(9):700–711.
5. Raichle ME (2011) The restless brain. *Brain connect* 1(1):3–12.
6. Buckner RL, Krienen FM, Yeo BT (2013) Opportunities and limitations of intrinsic functional connectivity MRI. *Nat Neurosci* 16(7):832–837.
7. Damoiseaux JS, et al. (2006) Consistent resting-state networks across healthy subjects. *Proc Natl Acad Sci USA* 103(37):13848–13853.
8. Greicius MD, Krasnow B, Reiss AL, Menon V (2003) Functional connectivity in the resting brain: A network analysis of the default mode hypothesis. *Proc Natl Acad Sci USA* 100(1):253–258.
9. Fox MD, Corbetta M, Snyder AZ, Vincent JL, Raichle ME (2006) Spontaneous neuronal activity distinguishes human dorsal and ventral attention systems. *Proc Natl Acad Sci USA* 103(26):10046–10051.
10. Smith SM, et al. (2009) Correspondence of the brain's functional architecture during activation and rest. *Proc Natl Acad Sci USA* 106(31):13040–13045.
11. Power JD, et al. (2011) Functional network organization of the human brain. *Neuron* 72(4):665–678.
12. Beckmann CF, DeLuca M, Devlin JT, Smith SM (2005) Investigations into resting-state connectivity using independent component analysis. *Philos Trans R Soc Lond B Biol Sci* 360(1457):1001–1013.
13. McKeown MJ, Hansen LK, Sejnowsk TJ (2003) Independent component analysis of functional MRI: What is signal and what is noise? *Curr Opin Neurobiol* 13(5):620–629.
14. McKeown MJ, Sejnowski TJ (1998) Independent component analysis of fMRI data: Examining the assumptions. *Hum Brain Mapp* 6(5-6):368–372.
15. Cole DM, Smith SM, Beckmann CF (2010) Advances and pitfalls in the analysis and interpretation of resting-state FMRI data. *Front Syst Neurosci* 4:8.
16. Beckmann CF (2012) Modelling with independent components. *Neuroimage* 62(2): 891–901.
17. Biswal BB, et al. (2010) Toward discovery science of human brain function. *Proc Natl Acad Sci USA* 107(10):4734–4739.
18. Fransson P, et al. (2007) Resting-state networks in the infant brain. *Proc Natl Acad Sci USA* 104(39):15531–15536.
19. Koch W, et al. (2010) Effects of aging on default mode network activity in resting state fMRI: Does the method of analysis matter? *Neuroimage* 51(1):280–287.
20. Yang Z, et al. (2014) Connectivity trajectory across lifespan differentiates the precuneus from the default network. *Neuroimage* 89:45–56.
21. Greicius MD, Srivastava G, Reiss AL, Menon V (2004) Default-mode network activity distinguishes Alzheimer's disease from healthy aging: Evidence from functional MRI. *Proc Natl Acad Sci USA* 101(13):4637–4642.
22. Jafri MJ, Pearlson GD, Stevens M, Calhoun VD (2008) A method for functional network connectivity among spatially independent resting-state components in schizophrenia. *Neuroimage* 39(4):1666–1681.
23. Greicius MD, et al. (2007) Resting-state functional connectivity in major depression: Abnormally increased contributions from subgenual cingulate cortex and thalamus. *Biol Psychiatry* 62(5):429–437.
24. Rocca MA, et al. (2012) Large-scale neuronal network dysfunction in relapsing-remitting multiple sclerosis. *Neurology* 79(14):1449–1457.
25. Piché M, et al. (2009) Characterization of cardiac-related noise in fMRI of the cervical spinal cord. *Magn Reson Imaging* 27(3):300–310.
26. Wei P, et al. (2010) Resting state networks in human cervical spinal cord observed with fMRI. *Eur J Appl Physiol* 108(2):265–271.
27. Xie G, et al. (2012) Reduction of physiological noise with independent component analysis improves the detection of nociceptive responses with fMRI of the human spinal cord. *Neuroimage* 63(1):245–252.
28. Barry RL, Smith SA, Dula AN, Gore JC (2014) Resting state functional connectivity in the human spinal cord. *eLife* 3:e02812.
29. Cadotte DW, et al. (2012) Plasticity of the injured human spinal cord: Insights revealed by spinal cord functional MRI. *PLoS ONE* 7(9):e45560.
30. Stroman PW (2009) Spinal fMRI investigation of human spinal cord function over a range of innocuous thermal sensory stimuli and study-related emotional influences. *Magn Reson Imaging* 27(10):1333–1346.
31. Stroman PW, Bosma RL, Tsyben A (2012) Somatotopic arrangement of thermal sensory regions in the healthy human spinal cord determined by means of spinal cord functional MRI. *Magn Reson Med* 68(3):923–931.
32. Stroman PW, et al. (2014) The current state-of-the-art of spinal cord imaging: Methods. *Neuroimage* 84:1070–1081.
33. Summers PEB, Brooks JCW, Cohen-Adad J (2014) Spinal Cord fMRI. *Quantitative MRI of the Spinal Cord*, eds Cohen-Adad J, Wheeler-Kingshott C (Academic, Amsterdam), pp 221–239.
34. Finsterbusch J, Eippert F, Büchel C (2012) Single, slice-specific z-shim gradient pulses improve T2*-weighted imaging of the spinal cord. *Neuroimage* 59(3):2307–2315.
35. Brooks JC, et al. (2008) Physiological noise modelling for spinal functional magnetic resonance imaging studies. *Neuroimage* 39(2):680–692.
36. Kong Y, Jenkinson M, Andersson J, Tracey I, Brooks JC (2012) Assessment of physiological noise modelling methods for functional imaging of the spinal cord. *Neuroimage* 60(2):1538–1549.
37. Brooks JCW, et al. (2012) Stimulus site and modality dependence of functional activity within the human spinal cord. *J Neurosci* 32(18):6231–6239.
38. Eippert F, Finsterbusch J, Bingel U, Büchel C (2009) Direct evidence for spinal cord involvement in placebo analgesia. *Science* 326(5951):404.
39. Filippini N, et al. (2009) Distinct patterns of brain activity in young carriers of the APOE-epsilon4 allele. *Proc Natl Acad Sci USA* 106(17):7209–7214.
40. Zuo XN, et al. (2010) Reliable intrinsic connectivity networks: Test-retest evaluation using ICA and dual regression approach. *Neuroimage* 49(3):2163–2177.
41. Kato G, et al. (2004) Electrophysiological mapping of the nociceptive inputs to the substantia gelatinosa in rat horizontal spinal cord slices. *J Physiol* 560(Pt 1):303–315.
42. Friesen WO, Cang J (2001) Sensory and central mechanisms control intersegmental coordination. *Curr Opin Neurobiol* 11(6):678–683.
43. Maieron M, et al. (2007) Functional responses in the human spinal cord during willed motor actions: Evidence for side- and rate-dependent activity. *J Neurosci* 27(15): 4182–4190.
44. Smith JC, Abdala APL, Borgmann A, Rybak IA, Paton JFR (2013) Brainstem respiratory networks: Building blocks and microcircuits. *Trends Neurosci* 36(3):152–162.
45. Dietz V (2003) Spinal cord pattern generators for locomotion. *Clin Neurophysiol* 114(8):1379–1389.
46. Goulding M (2009) Circuits controlling vertebrate locomotion: Moving in a new direction. *Nat Rev Neurosci* 10(7):507–518.
47. Grillner S, Jessell TM (2009) Measured motion: Searching for simplicity in spinal locomotor networks. *Curr Opin Neurobiol* 19(6):572–586.
48. Prut Y, Perlmutter SI (2003) Firing properties of spinal interneurons during voluntary movement. I. State-dependent regularity of firing. *J Neurosci* 23(29):9600–9610.
49. Aoki F, Wannier T, Grillner S (2001) Slow dorsal-ventral rhythm generator in the lamprey spinal cord. *J Neurophysiol* 85(1):211–218.
50. Soteropoulos DS, Edgley SA, Baker SN (2013) Spinal commissural connections to motoneurons controlling the primate hand and wrist. *J Neurosci* 33(23):9614–9625.
51. Cohen-Adad J, et al. (2010) BOLD signal responses to controlled hypercapnia in human spinal cord. *Neuroimage* 50(3):1074–1084.
52. Ko HY, Park JH, Shin YB, Baek SY (2004) Gross quantitative measurements of spinal cord segments in human. *Spinal Cord* 42(1):35–40.
53. Giove F, et al. (2004) Issues about the fMRI of the human spinal cord. *Magn Reson Imaging* 22(10):1505–1516.
54. Filippi M, Rocca MA (2013) Multiple sclerosis: Linking disability and spinal cord imaging outcomes in MS. *Nat Rev Neurol* 9(4):189–190.
55. Bot JC, Barkhof F (2009) Spinal-cord MRI in multiple sclerosis: Conventional and nonconventional MR techniques. *Neuroimaging Clin N Am* 19(1):81–99.
56. Cadotte DW, Fehlings MG (2013) Spinal cord injury: Visualizing plasticity and repair in the injured CNS. *Nat Rev Neurol* 9(10):546–547.
57. Smith SA, Pekar JJ, van Zijl PCM (2012) Advanced MRI strategies for assessing spinal cord injury. *Handb Clin Neurol* 109:85–101.
58. Woolf CJ (2011) Central sensitization: Implications for the diagnosis and treatment of pain. *Pain* 152(3, Suppl):S2–S15.
59. Finsterbusch J, Sprenger C, Büchel C (2013) Combined T2*-weighted measurements of the human brain and cervical spinal cord with a dynamic shim update. *Neuroimage* 79:153–161.
60. Jenkinson M, Bannister P, Brady M, Smith S (2002) Improved optimization for the robust and accurate linear registration and motion correction of brain images. *Neuroimage* 17(2):825–841.
61. Figley CR, Stroman PW (2007) Investigation of human cervical and upper thoracic spinal cord motion: Implications for imaging spinal cord structure and function. *Magn Reson Med* 58(1):185–189.
62. Verma T, Cohen-Adad J (2014) Effect of respiration on the B0 field in the human spinal cord at 3T. *Magn Reson Med* 72(6):1629–1636, 10.1002/mrm.25075.
63. Marrelec G, et al. (2006) Partial correlation for functional brain interactivity investigation in functional MRI. *Neuroimage* 32(1):228–237.
64. Smith SM, et al. (2011) Network modelling methods for FMRI. *Neuroimage* 54(2): 875–891.
65. Nichols TE, Holmes AP (2002) Nonparametric permutation tests for functional neuroimaging: A primer with examples. *Hum Brain Mapp* 15(1):1–25.